Proceedings of the Institution of Mechanical Engineers, Part D: Journal of Automobile Engineering
Volume 219, Number 4, 2005, 471-486

Aerodynamic investigations of ventilated brake disks

D. Parish and **D. G. MacManus***

Department of Aerospace Sciences, Cranfield University, Bedfordshire, UK

*Corresponding author. Dept. of Aerospace Sciences, School of Engineering, Cranfield University, Bedfordshire, MK43 0AL, UK.

Abstract:

The heat dissipation and performance of a ventilated brake disk strongly depends on the aerodynamic characteristics of the flow through the rotor passages. The aim of this investigation was to provide an improved understanding of ventilated brake rotor flow phenomena, with a view to improving heat dissipation, as well as providing a measurement dataset for validation of computational fluid dynamics (CFD) methods. The flow fields at the exit of four different brake rotor geometries, rotated in free air, were measured using a five-hole pressure probe and a hot-wire anemometry system. The principal measurements were taken using two-component hot-wire techniques and were used to determine mean and unsteady flow characteristics at the exit of the brake rotors. Using phase-locked data processing, it was possible to reveal the spatial and temporal flow variation within individual rotor passages. The effects of disk geometry and rotational speed on the mean flow, passage turbulence intensity and massflow were determined. The rotor exit jet and wake flow were clearly observed as characterized by the passage geometry as well as definite regions of high and low turbulence. The aerodynamic flow characteristics were found to be reasonably independent of rotational speed, but highly dependent upon rotor geometry.

Keywords: Brake disk, ventilated, aerodynamics, heat transfer, unsteady flow, turbulence.

Nomenclature

b	Brake rotor passage width, m
m	Mass flow, kg/s
m^*	Non – dimensional mass flow, $m/\rho U_2 A_2$
r	Radial distance, m
y	Circumferential distance, m
z	Axial distance, m
A	Brake rotor area, m^2
B	Brake rotor total width, m
BPF	Blade passing (frequency), Hz
C	Relative velocity, m/s
D	Brake rotor diameter, m
NB	Number of blades
Re_d	Reynolds number, $U_2 D_2/\nu$
Tu	Turbulence intensity, %
U	Blade speed, m/s
V	Absolute velocity, m/s
α	Absolute flow angle, degrees
β	Relative flow angle, degrees
ϕ	Flow pitch angle, degrees
ρ	Density, kg/ m^3
ν	Viscosity, m^2/s
ω	Rotational speed, rad/s

Subscripts

1	Brake rotor inlet
2	Brake rotor outlet
r	radial direction

1 INTRODUCTION

Automotive brakes are used to convert kinetic energy into thermal energy through friction between the brake pads and the rotor faces. If the brake disk temperatures become too high then the structural integrity will be compromised and the thermal load may lead to deformation, judder and increased wear. Although conventionally the cooling performance of the disk has been of less importance than other engineering aspects such as structural and manufacturing issues, improved heat dissipation will enable lighter, more reliable designs. A common method of enhancing the disk cooling is by using a ventilated brake rotor which improves the convective cooling by using air passages separating the braking surfaces. The rotor behaves as a centrifugal fan, drawing cool air from the inboard side, passing through the rotor passages and exhausting at the outer diameter. Ventilated brake rotor heat dissipation depends strongly on the aerodynamic behaviour of the flow through the rotor passages. All three mechanisms of heat dissipation contribute to the disk cooling, but it is anticipated that convection has a large impact for most ventilated rotor configurations. Conduction is frequently kept to a minimum in the design process to protect other components and the radiation terms only play a significant role at high temperatures [1].

The aerothermodynamics of a ventilated brake rotor is complex and highly dependent on the geometry of both the brake rotor and its surrounding environment. Although the aerodynamics of conventional centrifugal impellers has been extensively studied from a pumping performance and efficiency point of view [2, 3, 4, 5, 6], there has been very little work done on understanding the unusual aerodynamic design objectives for an automotive brake rotor where the dominant requirement is for cooling performance and thermal management. In addition, the brake rotor does not have the familiar turbomachinery inlet or outlet surrounding geometries and the operating point encompasses a broad range of rotating speeds. Clearly it is a field where the established turbomachinery knowledge base has a role to play but requires re-evaluation for the current applications.

Previous work has addressed both aerodynamic [1,7,8,9] and heat transfer [1,10,11], aspects for an assortment of ventilated and solid disks. Most previous workers measured the rotor exit airflow using pressure probes to measure the velocity profile and to calculate the rotor massflow. Barigozzi [7] is one of the few previous workers who used hot-wire anemometry (HWA) to examine the unsteady rotor exit flow field for two disk geometries featuring backward curved vanes and a pedestal arrangement. He showed that the pedestal configuration increased both the non-dimensional massflow as well as the reported turbulence intensity. Johnson [9] examined the flow field both surrounding the brake disc as well as inside the radial rotor passages using a two-component PIV system and, as anticipated, revealed large areas of separated flows within the passages. Other workers have shown that both local geometry modifications to the rotor inlet [8] and cross-drilled holes [11] can have a beneficial effect on the cooling performance. Computational studies have also been performed to examine the entire wheel arch area [12,13] as well as the brake rotor itself [1,15,16]. Voller [18] performed CFD analyses which showed good agreement between the experimental and predicted heat transfer coefficients for a range of rotational speeds and disk temperatures. Some workers have attempted to rank the relative importance of the mode of heat transfer and Limpert [11] suggests that internal convective cooling of ventilated rotors can contribute as much as 50 – 60% of total cooling at high rotor speeds. Conduction is limited by design to control the temperature of surrounding components and the cross-sectional area of the rotor is designed to prevent excess heat conduction to the wheel and hub. While attempts have been made to improve rotor-cooling performance, it is clear that the heat transfer phenomena and aerodynamic flow characteristics of the basic rotor geometry are not well understood. This is illustrated by the wide variety of rotor design improvements suggested by some of the work reported above.

The aim of this investigation is to provide an improved understanding of ventilated brake rotor flow features as well as to establish a CFD validation database. The flow at the exit of four different brake rotor geometries was measured using a five-hole

pressure probe and a hot-wire anemometer to determine mean and unsteady flow characteristics. The measurement of the unsteady velocity field using the hot-wire enabled phase-locked ensemble averaging to provide passage-to-passage velocity and turbulence intensity distributions at the exit of the brake rotors. This facilitates the identification of detailed flow features and comparisons between the different rotor designs and geometries. While it is appreciated that a brake rotor operating in free air is far from the true configuration, it was intended that this investigation would provide the first step in fully understanding the broader issues of brake rotor aerodynamics and cooling as well as providing a useful CFD validation database. In all of these experiments, no braking or thermal load was applied to the brake disk. Measurements were taken at a variety of radial distances from the rotor exit plane and at three rotational speeds (750, 1500 and 2250 rpm). The Reynolds number, based on the outside diameter and rotational speed, Re_Ω, ranged from 3.6×10^5 to 1.1×10^6.

2 EXPERIMENTAL APPARATUS

2.1 Test Pieces

The brake rotors were rotated using a mechanical lathe at up to 2250rpm and without forced convection in still, ambient air at room pressure and temperature. Four brake rotor geometries were tested as summarized in Table 1. Rotors 1, 2 and 4 featured backward curved vanes with a variety of diameters, passage numbers, passage widths and aspect ratios. The blade geometries are circular arc with squared-off leading and trailing edges. Rotor 3 is a different style of configuration which features internal pedestals and partial vanes. Full details of the geometry cannot be provided due to commercial confidentiality reasons.

2.2 Measurement Systems

The miniature five-hole pressure probe had an outside diameter of 1.5mm and was used to determine the mean flow properties such as yaw and pitch angle as well as mean velocity and massflow. It was primarily used as a preliminary measurement tool and also provided interesting comparisons with the hot-wire measurements. A constant

temperature hot-wire anemometry system (Dantec Streamline 90N10) was used to measure magnitude and direction of the velocity vector in the yaw plane, Figure 1. The Streamware system processes the raw voltage into velocity and decomposes the measured velocities into probe co-ordinates, using the manufacturers directional calibration coefficients. A Dantec 55P61 probe was used which has a tungsten wire of 5μm diameter with a low thermal inertia. Following the five-hole pressure probe surveys, the hot-wire was orientated so that the primary flow direction was set at approximately 45° to both sensors. Although the velocity components were simultaneously measured, the wires are off-set by about 1mm so that the measurements are not co-incident in space. An optical probe was used to provide a once-per-revolution which enabled phase locked data to be acquired.

To enable the results taken in the fixed frame of reference to be viewed appropriately in the rotating frame of reference, the measurement system must deliver sufficient data resolution per rotor vane passing. The hot-wire amplifier filter and gain were optimised to give an overall frequency response of 40kHz when tested in a representative airflow. Digital recording of the analogue signal provided by the hot-wire anemometer was performed using a National Instruments AT-MIO-16E-10 analogue to digital (ATD) converter, with a total sample rate of up to 100kS/s. A total of four input channels on the ATD card were occupied by the once-per-revolution optical sensor, the anemometer temperature probe and a separate channel for each of the two hot-wire signals. The sampling rate was set to 20kS/s per channel which established the measurement spatial resolution in the rotor frame of reference. The highest expected blade passing frequency, and corresponding lowest resolution, was for the 48 bladed rotor at 2250 rpm which equates to 1800Hz. Table 2 outlines the achieved points per rotor passage for each disk and rotational speed. With the sampling rate fixed at 20kHz, the Nyquist criterion dictates that the maximum expected resolved frequency is 10kHz. Although the achieved sampling rate was modest, the spatial resolution in the rotating frame of reference was still sufficient to discern the principal flow features.

2.3 Hot-wire calibration and uncertainty

The hot-wire calibration process requires the establishment of a relationship between the measured voltages and the flow velocity and direction. For this test the manufacturer's recommended directional calibration coefficients were deemed sufficient. This could be improved in further investigations by performing a full bespoke directional calibration for each individual probe. The velocity calibration was carried out using a dedicated calibration jet which delivered filtered, compressed air through a settling chamber to provide a low turbulence, flat velocity profile jet. The hot-wire probe was positioned one jet diameter downstream of the nozzle exit plane and a calibration was performed over the expected velocity range. During the experiments the temperature was simultaneously recorded and a correction applied if the temperature difference between calibration and experiment was greater than 5°C.

As with all measurement techniques the final error depends on the chain of systems each of which will have its own systematic and random type errors. It is difficult to provide a comprehensive error assessment although this type of hot-wire measurement technique is well established. A brief summary of the main error sources is provided for completeness. The calibration jet velocity was determined from a digital manometer which was estimated to be accurate within ±2% over the range of interest. The hot-wire probe was positioned with the wires at 45° to the calibration jet by measurement. This was estimated to have an error margin of ±1°. Curve fitting of the resulting calibration data yielded results to within ±0.7%. Jorgensen [17] suggests that commercially available anemometers have low drift, low noise and good repeatability, which does not add significantly to the experimental uncertainty. Probe initial positioning relative to the brake disk was estimated to have an uncertainty of ±0.2mm. Traversing was carried out using the lathe digital measuring system, which had an accuracy of 0.01mm. Temperature variations were corrected by using the anemometer's built-in temperature correction facility and are not thought to have contributed significantly to the uncertainty.

3 MEASUREMENTS

3.1 Introduction

Given that the brake rotor acts as an impeller, there is much to be gleaned from the broad knowledge base of turbomachinery aerodynamics when examining the current flow fields. A conventional impeller flow field is very complex and has been explored both experimentally and computationally by a variety of workers [2, 4, 19, 20, 21]. The flow is usually highly three-dimensional and unsteady with regions of separated flow at some operating points. In addition, it is susceptible to secondary flow patterns due to Coriolis and gyroscopic forces as well as the flows driven by radial equilibrium and cross-passage pressure gradient terms [3]. One of the dominant features for an impeller flow field is the jet and wake flow pattern as well as the possibility of large flow separations leading to significant flow blockage and non-uniform mass distributions.

Pressure measurements were taken using a five-hole probe along axial traverses at a range of radial positions at the rotor exit (Figure 1) for all four rotors. Hot-wire axial traverses were performed at a fixed circumferential location and at the closest radial position, 2mm from the exit plane, for Rotors 2, 3 and 4. The measurement domain extended beyond the plane of the rotor by about 6mm on both the inboard and outboard sides and data was taken at 1.0mm axial intervals which typically gave 30 points across the domain. The hot-wire measurements were taken over 100 revolutions and ensemble averaged based on the once-per-revolution (OPR) signal from the optical probe. The measurements provided mean and unsteady data for the radial and circumferential velocities in the absolute frame of reference. Relative velocity and whirl angle were subsequently determined by taking the rotational velocity into account.

3.2 Spectral analysis

The frequency power spectrum was calculated for each of the measurement sets, based on the rotor relative velocity. The highest blade passing frequency was 1800Hz (48 blades at 2250rpm), although there was no significant measured frequency content

above 5000Hz for all of the rotors. This gave confidence that the measurement system had the capability to measure primary details of the flow field. For all rotors, the fundamental blade passing frequency (BPF) was clearly observed and for some configurations up to the sixth harmonic of the BPF was also measured (Figure 2). Just as the fundamental BPF reflects the passing of a sinusoidal jet-wake perturbation, then the higher harmonics represent higher spatial frequency within the rotating blade passage. Figure 2 shows a high harmonic content because it has the lowest number of passages which means that the rotor exit flow field has a greater spacing between the wakes, is less of a simple sinusoid in shape and therefore contains higher spatial frequency. For most of the rotors, the exit flow field is dominated by the jet-wake flow pattern and, as expected, the spectral power decreases strongly for these higher harmonics. Figure 2 also shows that Rotor 4 exhibits a sub-harmonic unsteadiness at ½ BPF (300Hz). This is due to the fixing arrangement of the impeller where the inlet to every second passage is partially obscured by a bolt head. Similar effects were observed on the other rotors where every fourth passage was partially obstructed and the spectral frequency showed a peak at ¼ BPF.

3.3 Circumferentially Averaged Results

Circumferential averages for the velocities and flow angles were calculated from the data measured over 100 revolutions which highlighted some basic features of the aerodynamics. Overall, the rotor measurements (both five-hole probe and hot-wire) showed that, the exit flow angles, both relative and absolute, are predominately insensitive to rotational speed. In addition, the absolute and relative velocities primarily vary linearly with rotational speed and the velocity and massflow axial distributions do not significantly change across the operating range of 750 to 2250 rpm. This highlights the point that over most of the measured rotational speed range, the aerodynamic flow features of the rotor are unchanging. For example, Figure 3(a)-(d), shows the absolute angle (α), relative angle angle (β),non-dimensional relative velocity and radial velocity for Rotor 2 for rotational speeds of 750, 1500 and 2250 rpm. There are only minor changes in the flow between 1500 and 2250 rpm and the largest differences occur at

the lowest speed. This is evident in the relative flow angle and relative velocity, Figure 3(b)-(c). It also shows that at the lowest speed the brake rotor has a slightly higher non-dimensional velocity and provides turns the flow through a greater angle in the relative frame of reference i.e. lower exit relative flow angle β_2. The radial velocity is a direct measure of the rotor massflow and shows the distribution across the passage span, Figure 3(d). There is a small decrease in the non-dimensional radial velocity at the lowest rotational speed which is consistent with the increased relative velocity exiting at a lower relative flow angle. The massflow peak is consistently located towards the outboard side of the disk. This is probably due to a separation at the inlet where the flow has to turn 90 degrees from axial to radial across a sharp cornered geometry. The maximum non-dimensional radial velocity (and massflow) for this case is achieved at 1500 rpm although the axial distribution does not change significantly. Figure 1 includes an illustrative schematic of the mid-span velocity triangles at the rotor exit.

Comparisons of the circumferentially averaged exit flows for the different Rotors (2, 3 and 4) are presented in Figure 4(a)-(e). The measurements were taken 2mm from the rotor exit plane at 1500rpm. Overall, the trends and levels are reasonably similar for the different designs – which is not too surprising given the common dimensions of diameter, passage height and blade exit angle (Table 1). The main difference in geometry is the different number of passages (Rotor 2 and Rotor 4) as well as the part-span vanes and pedestals of Rotor 3. One of the most notable features is the improved uniformity in the inboard region (z/b = 0.5-1.0) for Rotor 3 in terms of the relative angle and non-dimensional velocity (Figure 4(b), (d)). This may be due to the more complicated and irregular geometry of Rotor 3 preventing the formation of a large separation region and the pedestals encouraging mixing of the flow and redistribution of the massflow. Figure 4(e) compares the radial velocity distributions for each of the rotors and highlights the more uniform massflow distribution delivered by Rotor 3 - particularly in the inboard region which is expected to improve the cooling performance on the inboard face.

3.4 Rotor massflow

An important parameter when considering the cooling performance of a brake disc is the mass flow rate which the impeller draws through the rotor passages. The rotor average massflow was calculated from the radial velocity component and was non-dimensionalised based on the exit rotation speed, U_2, a reference density and a total geometric passage exit area ($m^* = m/\rho U_2 A_2$). Overall, the non-dimensional massflow flow varies only slightly with rotational speed indicating that the rotor aerodynamics do not radically change at the different operating points (Figure 5). This is in agreement with previous workers who showed a linear trend of massflow with rotational speed [1,8,10]. However, there is a modest deviation in Rotor 2 which shows a maximum non-dimensional massflow at 1500rpm followed by a very small decrease at 2250rpm. Another significant aspect is the comparison between the different rotor designs which show that, relative to Rotor 2, Rotors 3 and 4 deliver up to 25% and 45% more massflow, respectively. All three rotors have essentially the same diameters, passage width and vane thickness (Table 1) and the only significant changes are in the number and design of the passages. Comparing Rotors 2 and 4 shows the effect of reducing the number of rotor blades from 48 (Rotor 2) to 24 (Rotor 4). The large change in massflow could be due to a range of effects but the primary influences are expected to be due to the change in passage aspect ratio and the reduction in inlet geometric blockage. The increased passage area means that for the same blade length the boundary layers and wake regions are, to a first order, proportionally smaller. In addition, the reduced number of leading edges at the inlet reduces the geometric blockage as both rotors have the same approximate vane thickness. Although increasing the massflow increases the potential cooling available to the rotor, it does not necessarily mean that the rotor cooling is improved as its benefits are offset by the reduction in surface area, and the overall performance will also depend on the detailed massflow distribution within the passage, turbulence intensity as well as other mechanical constraints. Although Rotor 3 has similar overall dimensions to Rotors 2 and 4, the geometry of the vanes is very different with nominally 36 passages which

include part-span turning vanes as well as mid-passage pedestals. Nevertheless, Rotor 3 delivers more massflow than Rotor 2 and at 1500rpm is only 5% below the Rotor 4 peak massflow. On this basis it appears that Rotor 2 is over bladed which is restricting the massflow and that the complex geometry of Rotor 3 has a beneficial effect on both the massflow level and axial distribution. This will be referred to later on when the effect of the Rotor 3 geometry on the turbulence characteristics will also be examined.

3.5 Comparison between hot-wire and five-hole probe measurements.

The pneumatic pressure probe used in this, and most previous experiments, has a very low frequency response. The probe measures "quasi-steady" changes in total pressure and was calibrated for yaw, pitch and magnitude in a reference known flow and velocity was determined by assuming that the exit flow was at atmospheric static pressure. As discussed in §2.3, the hot-wire velocity magnitude calibration was performed using a calibration jet and the manufacturers geometric transformation to resolve into the required velocity components. Overall, the measurement systems were calibrated completely independently of each other.

Figure 6(a) compares the absolute exit yaw angle measured by the five-hole probe with the circumferentially average hot-wire results for Rotor 2 at 1500rpm. The results are in very good agreement with the largest difference of about 3°. However, a comparison between the measured absolute velocity shows significant differences between the pressure probe and the hot-wire (Figure 6(b)), where on average the magnitude of the hot-wire results are about 75% of the pressure based measurements. This could be due to a wide range of issues such as calibration differences or processing errors. However, there are a variety of aspects worth considering which could have resulted in an artificially high mean velocity for the pressure based data. The miniature 5-hole probe had a diameter of 1.5mm relative to the passage height of 19.5mm and although the jet is unbounded, there may be a local blockage effect which would result in an increased velocity reading from the pressure probe. Also, although

the pressure probe was only 2mm from the disc edge, it was assumed that the flow was at atmospheric static pressure. Another contributing factor may be due to the highly unsteady nature of the flow field due to both instantaneous turbulence as well as deterministic wake-jet passing events. The five-hole probe has a very low frequency response and it is known [22] that high levels of flow unsteadiness can result in artificially high readings of total pressure and consequently velocity. This argument is supported by the better agreement which is obtained in the inboard and outboard regions where both the 'turbulence' and deterministic unsteadiness is very low. Also, the good agreement in the yaw angle results is due to only small angle deviations between the jet and the wake as will be presented later on from the hot-wire measurements. Many previous workers have used five-hole probes as a way of measuring the rotor massflow but these results indicate that such methods may be unreliable and prone to over-estimating the massflow.

3.6 Frame of reference

An ensemble averaged flow field was constructed from 100 revolutions which enabled the average variation of absolute velocity and whirl angle in each separate blade passage to be examined. For example, Figure 7(a) shows the regular, periodic variation of absolute velocity over six individual blade passages for Rotor 2 at 2250rpm. A better understanding of the individual passage aerodynamics is obtained by transforming the results into the relative frame of reference. Figure 7(b) is the corresponding relative velocity distribution which clearly shows the jet and wake flow structure associated with each rotor passage. It is interesting to note that due to the high rotational speed relative to the flow speeds, the regions of high *absolute* velocity correspond to the rotating wake regions where there are low *relative* velocities. This is illustrated in Figure 8 which shows a schematic of the mid-passage velocity triangles for both jet and wake regions. The transformation into the relative frame of reference also accentuates the passage flow structure. Figure 7(c) highlights the modest changes in relative flow angle between the mainstream and wake regions. However,

the combination of changing relative angle and relative velocity results in substantial changes in the absolute flow angle (Figure 8).

3.7 Ensemble averaged passage results

Processing of the unsteady measurements into the relative frame of reference enables interpretation of the ensemble averaged rotor flow field and comparisons to be made between the different brake disk designs. Figure 9 shows the relative velocity distributions for Rotors 2, 3 and 4 along with schematics of the rotor geometries for Rotor 2 and 4. For all rotors, the basic jet and wake structure is clearly identifiable along with some significant differences between the rotors. From Figure 9(a)-(c) it is apparent that, as expected, the high velocity jet or mainstream flow is closer to the pressure side (PS) of the rotor passage and that the low-velocity wake region is towards the suction side (SS). In addition, the overall flow is skewed towards the outboard side of the passages for all the rotors. This was previously noted in §3.4 and is probably due to a separation at the inlet where the flow negotiates a 90 degree turn from axial to radial. For Rotor 2 (Figure 9(a)) the wakes and jets are curved away from the direction of rotation (as presented the disk rotation is from right to left). This is probably due to the secondary flows and asymmetric boundary layer growth as mentioned in §3.1. The results also show the additional blockage in terms of lower peak velocity for the passages where the inlet is obstructed by the fixing bolt. This confirms the spectral plots presented in §3.2. This also applies to Rotor 3 and Rotor 4 where the main effect is due to the balancing clip as shown in the geometry schematic,Figure 9(b)-(c). Comparing Figure 9(a) and (c) highlights the effect of changing the number of rotor vanes from 48 to 24. The mainstream jet portion of the flow in Figure 9(c) is much larger than Figure 9(a) and although the wakes have about the same velocity deficit, they encompass a much smaller proportion of the flow field. This reflects the increased massflow rate for Rotor 4 as presented in Figure 5.

The flow field for Rotor 3 (Figure 9(b)) is characteristically different from the other two configurations. The wake regions are proportionally bigger and exhibit a different

shape. This is due to the presence of part-span pedestals which are generating additional wake flows near both endwalls. Also in evidence is the region where the mainstream jet narrows as it passes through the mid-height channel created by the partial pedestal on each endwall. This accounts for the change in shape of wake, which now occupies a more significant portion of the flow in the important endwall regions. As with the more conventional Rotor 2, Figure 9(a), the effect of the blockage due to the fixing bolt heads is seen in passages 1 and 4 (y/b ~ 2 and 7).

Overall, there are only modest changes in the relative yaw angle and for the datum Rotor 2, at the mid-span location, the angle varied from 28° close to the wake region and approximately 24° in the jet region. This reflects the underturning (high β_2) experienced by the low-momentum regions. The largest gradients of yaw angle are between the mid-passage regions and the endwall flows where the relative exit angles are very low. In these regions the relative velocity is reasonably high but there is very little radial throughflow and the relative flow angles are therefore low. The relative whirl angles in the jet regions are reasonably close to the idealized value with very little slip between the flow and the rotor metal exit angle. The radial velocity contours for each of the rotors, Figure 10(a)-(c), reiterate the primary observations such as the skewed massflow distribution towards the outboard side and the localised blockage effects of the mounting bolts and balancing clips. This is particularly evident in Figure 10(b) which shows the massflow reduction due to the bolt in every fourth passage (y/b ~ 2 and 7).

3.8 Turbulence characteristics

It is well established that the use of flow turbulators (pins, pedestals, ribs etc) can significantly enhance the heat transfer for internal passages (23). This type of technology has been particularly applied to gas turbines where the average surface heat transfer coefficients can be increased by up to a factor of 2.8. For turbine applications this typically increased the required pumping power by up to a factor of 10

(23,24). Clearly, this type of technology could play an important role in enhancing the brake disk cooling performance and some designs already include pedestal geometries. Although this experiment does not measure the heat transfer coefficients or the detailed internal flow regimes, an examination of the unsteady exit flow field may prove instructive. From the 100 revolutions of recorded unsteady data the ensemble averaged relative velocities, C', corresponding to each rotor circumferential location was determined. This averaged periodic flow field was subtracted from each revolution dataset to provide a flow unsteadiness term, C'', at each location for the individual rotor passages. The root-mean-square of C'' was used to calculate a "turbulence intensity" term, Tu, as follows:

$$Tu\% = \frac{\sqrt{\overline{C''^2}}}{C'} \cdot 100$$

Even though referred to as "turbulence intensity", this term is more accurately described as a non-deterministic unsteadiness and quantifies the flow variations which are not at blade passing frequency. Although the sample size of 100 revolutions is modest for determining "turbulence" data, the results were consistent and repeatable which gave some confidence in the presented measurements. To resolve the unsteady data into the rotating frame of reference, it is vital that the velocities were measured simultaneously although for this two-component hot-wire, this does mean that there is a spatial offset between the measured components due to the wire construction of 1mm. Nevertheless, the results obtained are instructive and provide useful data for comparing the characteristics of the different rotor designs. The term *turbulence* is used here as a matter of convenience although it is sometimes interchanged with the term *unsteadiness*.

Figure 11(a)-(c) shows the measured turbulence intensity, Tu, distributions for Rotor 2, 3 and 4. When compared with Figure 9(a)-(c), it is clear that the regions of high turbulence coincide with the low relative velocity wake regions. The mainstream

jet regions of the passage flows exhibit much lower turbulence levels. This is as expected and has been observed in both conventional turbomachinery flows [25,26] as well as other brake disk investigations [7]. The wake regions predominately comprise of the vane and endwall turbulent boundary layers which are augmented by vortex shedding, wake oscillations and unsteadiness of the separation points. Previous studies have also revealed a very unsteady flow field at the impeller exit [9]. In this example, Figure 11(a) shows that the wake flow on Rotor 2 has a peak turbulence intensity of about 20% whereas the mainstream jet has a very low level of less than 2%. In addition, it also shows that the fixing bolt head has increased the passage mainstream turbulence distribution (e.g. y/b ~ 2 and 7). The effect of reducing the number of blades from 48 (Rotor 2) to 24 (Rotor 4) has no significant impact on the general turbulence characteristics, Figure 11(a) and (c). The wake regions have a slightly higher peak turbulence levels (24%) and the mainstream flows are slightly lower (1-2%). The higher peak turbulence level relative to Rotor 2 may be due to increased endwall driven secondary flows within the rotor passage as the number of vanes has been reduced from 48 to 24. Similar to the effect of the fixing bolt head on Rotor 2, the balancing clip on Rotor 4 (see Figure 9) increases the average mainstream turbulence level for the locally affected passages (y/b ~ 6-8) to about 5-8%. These effects are as expected and simply highlight the additional wakes and disturbances introduced into the flow.

Although Rotors 2 and 4 are reasonably similar, Rotor 3 is characteristically different, Figure 11(b). It was specifically designed with the intention of improving the brake cooling performance by increasing the turbulence through the introduction of part-span vanes and pedestals. Figure 11(b) shows that although the peak turbulence levels are similar to Rotors 2 and 4, the extent and distribution of the high turbulence regions have increased significantly. This is similar to the changes in the mean relative flow field presented in Figure 9. An additional important change is the increase in turbulence levels in the regions closest to the passage endwalls where the heat transfer is required the most. Comparing Figure 11(a) and (b), shows that for Rotor 3,

the endwall turbulence levels are higher - particularly on the inboard face (z/b = 1) where there is about a 50% increase. Figure 12 shows the distribution of the circumferential averages of the turbulence intensity for Rotors 2, 3 and 4. The traverse extends beyond the disk width and the outer faces of the endwalls correspond to z/b = 0 and 1, respectively. The plot clearly shows the increased turbulence intensity of Rotor 3, reaching on average 4% turbulence points greater than Rotor 2. The distribution highlights the average increase in the turbulence intensity for Rotor 3 at the inboard passage wall (z/b=1), indicating the potential for improved heat transfer. The distribution of Rotor 3 also shows a double peak, which is likely to be due to the low turbulence jet being forced into the centre of the passage by the part-span pedestals.

The passage-to-passage distributions of flow and turbulence through the datum brake rotor passages is far from uniform, which will lead to high and low temperature regions during vehicle braking. This is undesirable as thermal stresses are created within the material. The turbulence of the flow through Rotor 3 was shown to increase relative to the standard bladed rotors, indicating that heat transfer is likely to be greater in this case. This is an important result, as the rotor geometry increases overall turbulence intensity, without significantly reducing the mass flow or relative velocity. The surface area of the internal passage is also increased due to the pedestal arrangement, which suggests that this brake rotor may provide increased heat dissipation. Overall, Rotor 3 is delivering a massflow and flow field characteristics which are expected to improve the convective cooling of the brake disk. This is supported by unreported tests which have shown that, under a known braking load, Rotor 3 performs better than the other designs and has lower peak temperatures.

4 CONCLUSIONS

The unsteady flow fields of a variety of ventilated brake rotor disks were measured using a two-component hot-wire anemometer to determine the mean and unsteady velocity and whirl angle distributions at the rotor exit plane of a brake disk impeller. The measurements revealed the detailed flow structures, and enabled the exit flow fields of

individual blade passages to be examined. The time-averaged measurements show that the rotor aerodynamic behaviour, as reflected in the exit angle and non-dimensional velocities, is not significantly affected by rotational speed. In addition, the rotor massflow is shown to vary approximately linearly with rotational speed. For these particular brake discs it was found that a reduction in the number of vane passages increased the delivered massflow. Comparisons between hot-wire measurements and pressure probe data, show good agreement in terms of flow angle but demonstrate the inability of the pressure probe to capture the wake regions and the consequent overestimation in flow rate.

The passage-to-passage wake-jet flow is found to be a characteristic signature of the exit flow field with large unsteadiness in the wake region compared to the mainstream flow. These flow patterns are affected by local geometric features which influence the massflow and turbulence distributions. Although, the number of vane passages has a primary effect on the massflow, it has only a modest effect on the turbulence characteristics for each passage. However, the addition of pedestals and part-span turning vanes has a dramatic effect on the flow by changing the turbulence distributions. Although the peak levels are unaffected, the mean turbulence increases by approximately 50% relative to the datum geometry. These local geometric features also result in more uniform massflow and turbulence distributions along with a marked improvement towards the inboard endwall. In addition, these enhancements are achieved without any significant deterioration in the total massflow.

5 ACKNOWLEDGEMENTS

The authors would like to acknowledge the help of the workshop and technician staff at the School of Engineering, Cranfield University.

REFERENCES

1. Sisson, A. E., Thermal analysis of vented brake rotors, *SAE Paper 780352*, 1978.

2. Cumpsty, N.A., *Compressor aerodynamics*, Longman Group, Harlow, 1989.

3. Lakshminarayana, B., *Fluid dynamics and heat transfer of turbomachinery*, Wiley and Sons, New York, 1996.

4. Japikse, D., *Introduction to turbomachinery*, Concepts ETI, Vermont USA, 1997.

5. Wilson, D., Korakianitis, T., *The design of high-efficiency turbomachinery and gas turbines*, 2nd Edition, Prentice Hall, 1998.

6. Whitfield, A., Baines, N.C., *Design of radial turbomachines*, Longman Scientific and Technical, New York, 1990.

7. Barigozzi, G., Cossali, G. E., Perdichizzi, A., Boden, A., Pacchiana, P., Experimental investigation of the mean and turbulent flow characteristics at the exit of automotive vented brake discs, *SAE Paper 2002-01-2590*, 2002

8. Hudson, M. D. and Ruhl, R. L., Ventilated Brake Rotor Air Flow Investigation, *SAE Paper 971033*, 1997.

9. Johnson, D., Sperandei, B., Gilbert, R., Analysis of the flow through a vented automotive brake rotor, *Journal of Fluids Engineering*, Vol. 125, pp. 979-986, November 2003.

10. Limpert, R., Cooling Analysis of Disc Brake Rotors, *SAE Paper 751014*, 1975.

11. Limpert, R., Thermal Performance of Automotive Disc Brakes, *SAE Paper 750873*, 1975.

12. Shen, F. S., Mukutmoni, D., Thorington, K. and Whaite, J., Computational flow analysis of brake cooling, *SAE Paper 971039*, 1997.

13. Krüsemann, R. and Schmidt, G., Analysis and optimisation of disk brake cooling via computational fluid dynamics, *SAE Paper 950791*, 1995.

14. Daudi, A. R., 72 curved fins and air director idea increases airflow through brake rotors, *SAE Paper 1999-01-0140*, 1999.

15. Zhang, J. J., A high aerodynamic performance brake rotor design method for improved brake cooling, *SAE Paper 973016*, 1997.

16. Bleier, F. P., *Fan handbook – selection, application and design*, McGraw-Hill, Maidenhead, 1997.

17. Jorgensen, F. E., *How to measure turbulence with hot-wire anemometers – a practical guide*, Dantec Dynamics, 2002.

18. Voller, G., Tirovic, M., Morris, R., and Gibbens, P., Analysis of automotive disc brake cooling characteristics", *Proc. Instn. Mech. Engrs.,Part D: Journal of Automobile Engineering*, Vol 217, pp. 657-666, 2003.

19. Eck, B., *Fans – design and operation of centrifugal, axial-flow and cross-flow fans*, Pergamon Press, Oxford, 1973.

20. Krain, H., Swirling impeller flow, *Journal of Turbomachinery*, Vol. 110, 1988.

21. Hathaway, M., Chriss, R., Wood, J., and Strazisar, A., Experimental and computational investigation of the NASA low-speed centrifugal compressor flow field, *Journal of Turbomachinery*, Vol. 115, pp. 527-542, 1993.

22. Goldstein, R.J., Fluid Mechanics Measurements, Hemisphere Publishing, 1983.

23. Han, J., Dutta, S., Ekkad, S., *Gas turbine heat transfer and cooling technology*, Taylor and Francis, New York, 2000.

24. Bunker, R., Wetzel, T., Rigby, D., Heat transfer in a complex trailing edge passage for a high pressure turbine blade - Part 1: experimental measurements, *GT-2002-30212, International gas Turbine Conference and Exposition*, Amsterdam, 2002.

25. Akhras, A., El Hajem, M., Morel, R., Champagne, J., The internal flow investigation of a centrifugal pump, *Proc. 10th International Symposium on Application of Laser Techniques to Fluid Mechanics*, Lisbon, 2000.

26. Ubaldi, M., Zunino, P., Ghiglione, A., Detailed flow measurements within the impeller and the vaneless diffuser of a centrifugal turbomachine, *Experimental Thermal and Fluid Science*, Vol. 17, pp.147-155, 1998.

	Rotor 1	Rotor 2	Rotor 3	Rotor 4
Outer Diameter (m)	0.33	0.37	0.366	0.37
Inner Diameter (m)	0.222	0.274	0.274	0.274
Total Thickness (m), B	0.028	0.032	0.032	0.032
Passage Height (m), b	0.016	0.0195	0.019	0.019
Area at inlet (m^2), A_1	0.0112	0.0168	0.0164	0.0164
Area at outlet (m^2), A_2	0.0166	0.0227	0.0218	0.0221
Number of Blades, NB	48	48	36	24

Table 1 Rotor geometry specifications.

Rotational speed (rev/min)	**2250**	**1500**	**750**	**1500**	**1500**
Rotor #	2	2	2	3	4
Number of blades	48	48	48	36	24
BPF, Hz	1800	1200	600	900	600
Sample points per blade pitch	11	17	33	22	33

Table 2 Estimated spatial resolution in the rotating frame of reference. Sample rate of 20kHz.

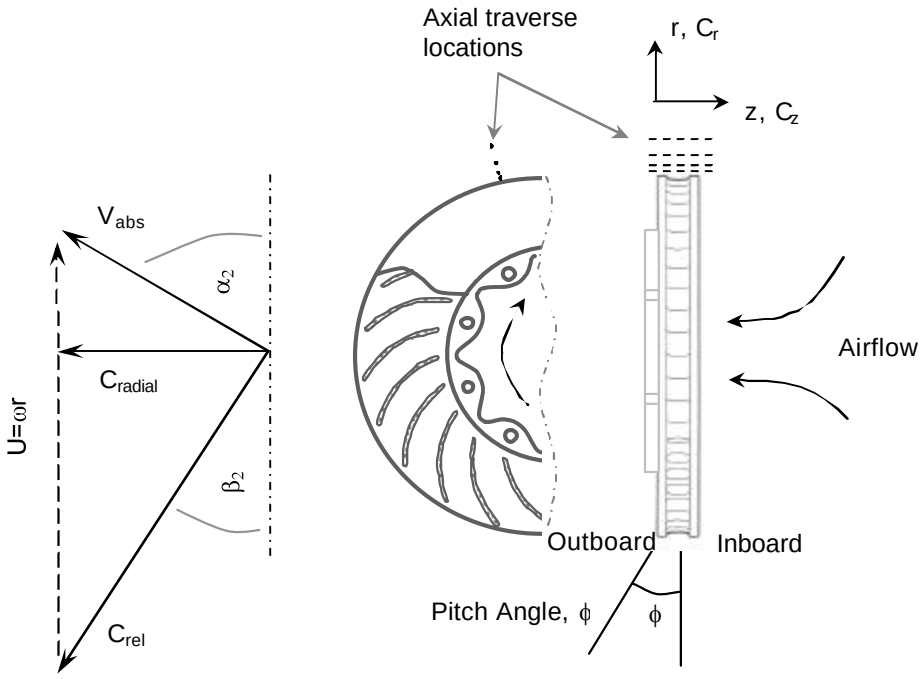

Figure 1 Definition of measurement coordinate system and schematic of exit velocity triangles

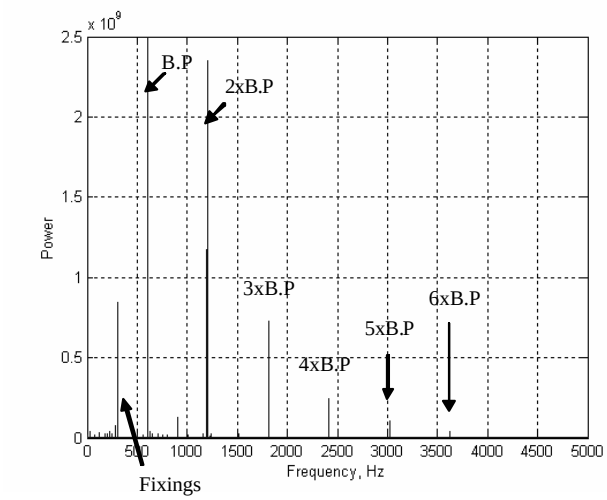

Figure 2 Power spectral density at rotor exit. Rotor 4. 2mm from exit plane. Mid-passage axial location, 1500 rpm.

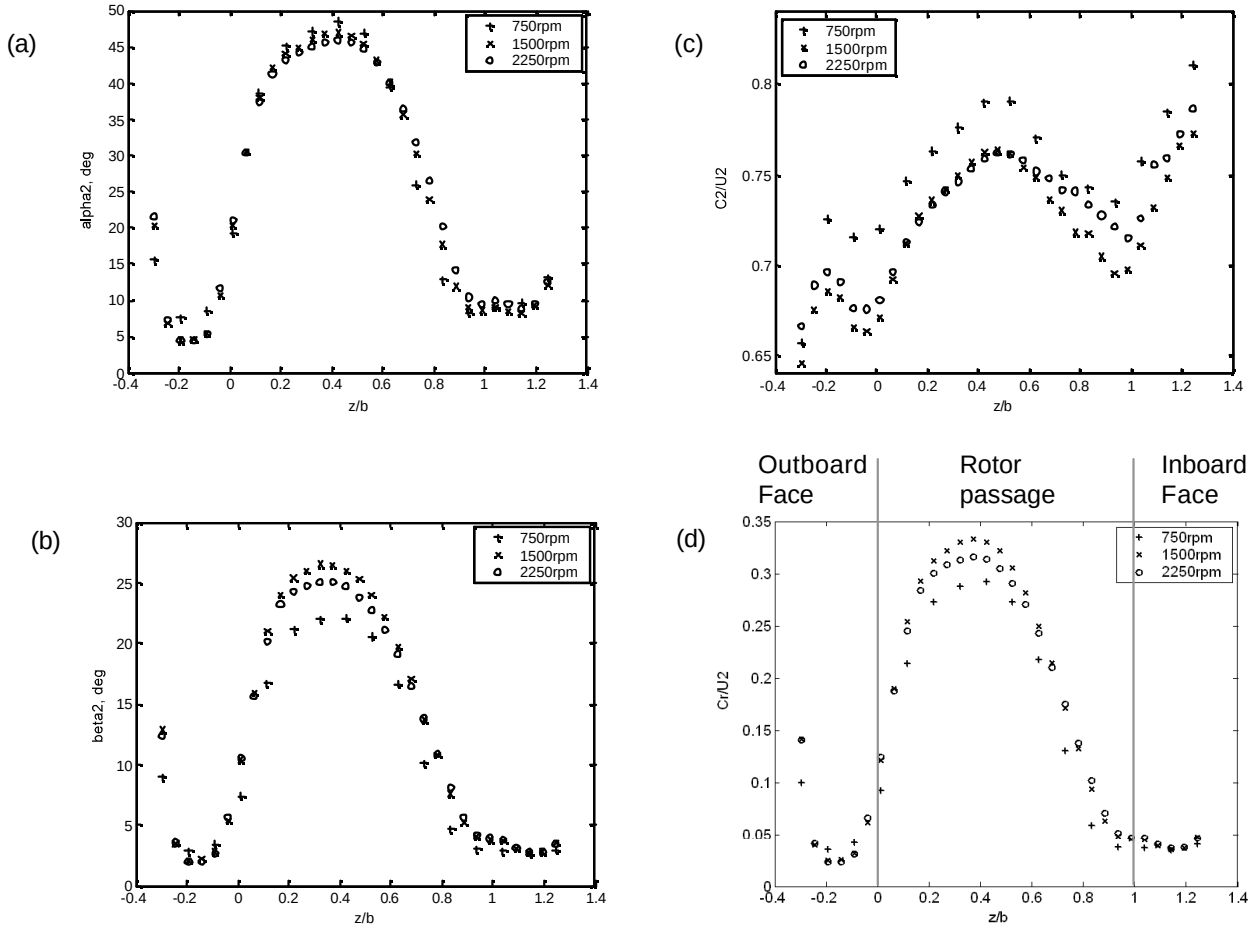

Figure 3 Circumferentially averaged (a) absolute yaw angle (b) relative yaw angle (c) relative velocity (d) radial velocity. Rotor 2 at 750, 1500 and 2250 rpm. Traverse taken 2mm from the rotor exit.

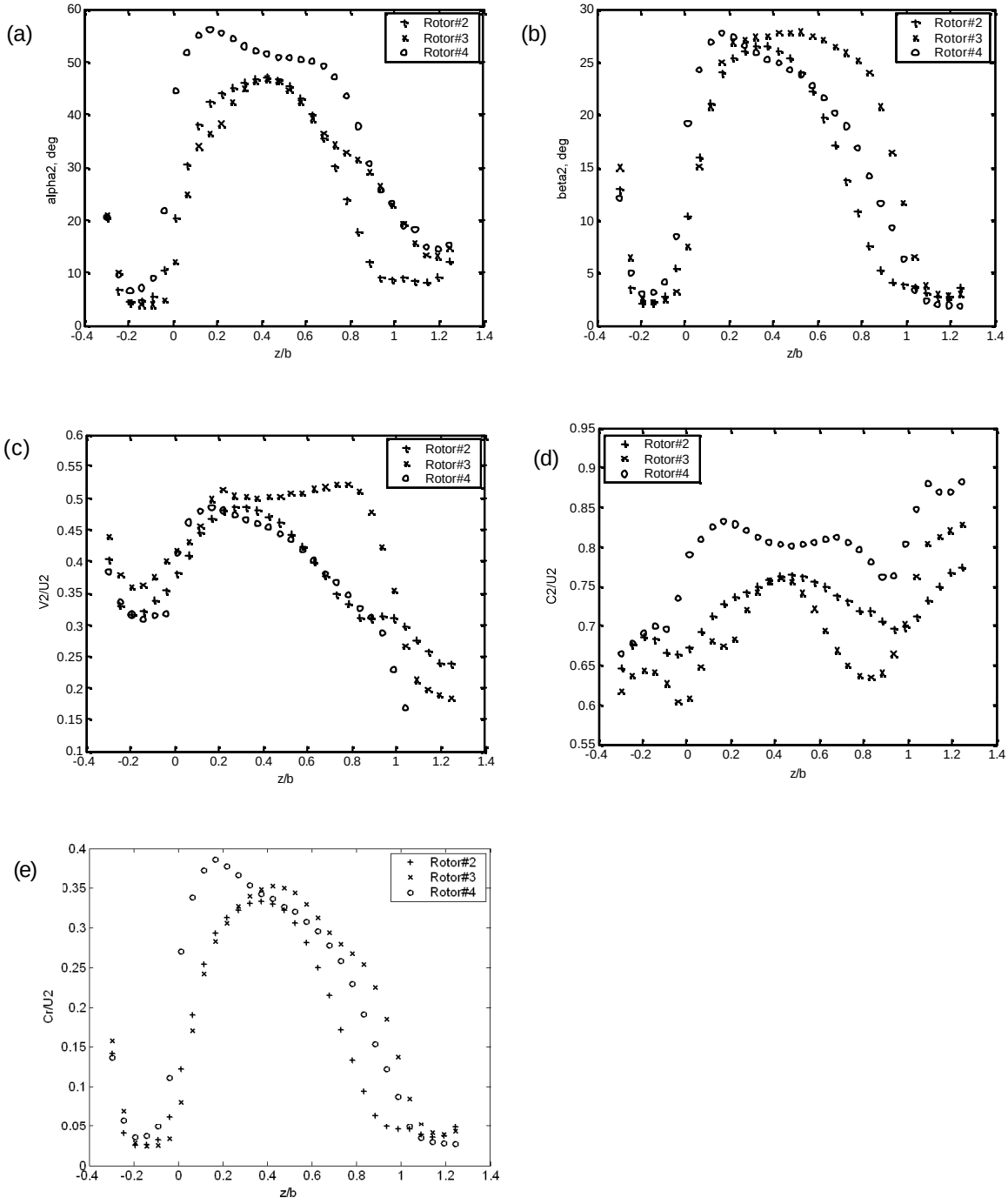

Figure 4 Circumferential averages (a) absolute angle (b) relative angle (c) absolute velocity (d) relative velocity (e) radial velocity for Rotors 2, 3 and 4 at 1500RPM.

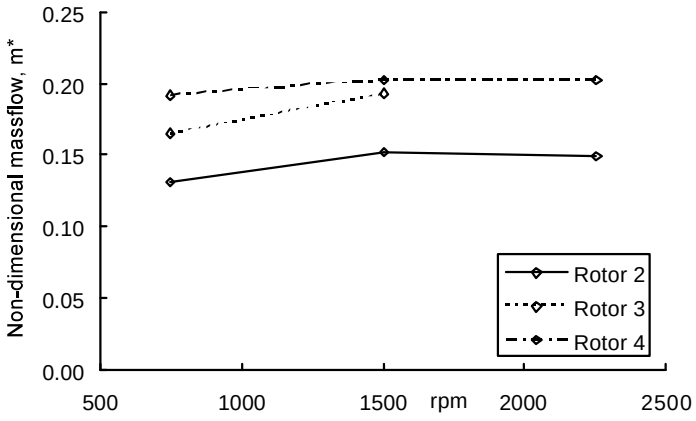

Figure 5 Non-dimensional massflow as a function of rotational speed.

(a)

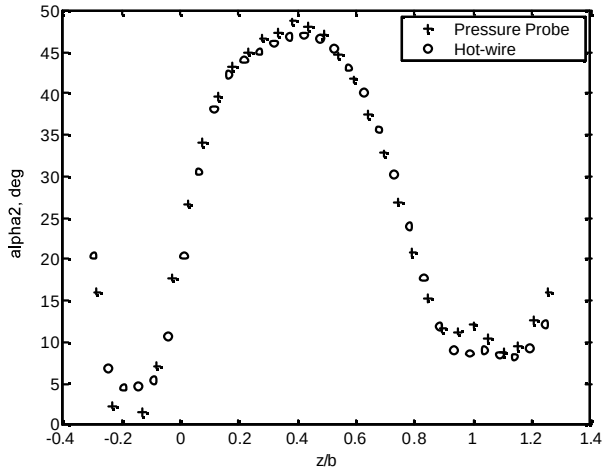

(b)

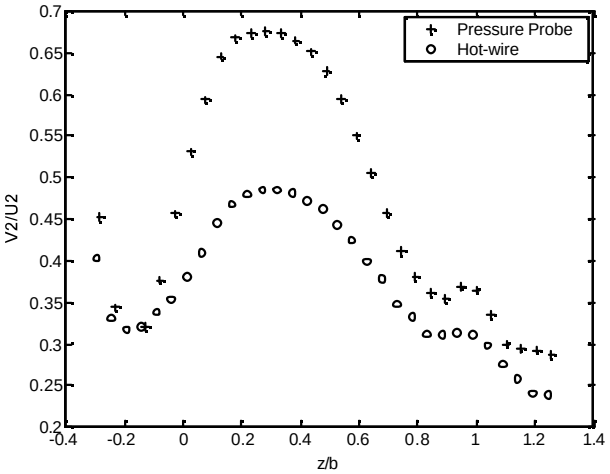

Figure 6 Comparison between hot-wire and five-hole pressure probe measurements for (a) absolute whirl angle and (b) absolute velocity. Rotor 2, 1500rpm, 2mm from exit plane.

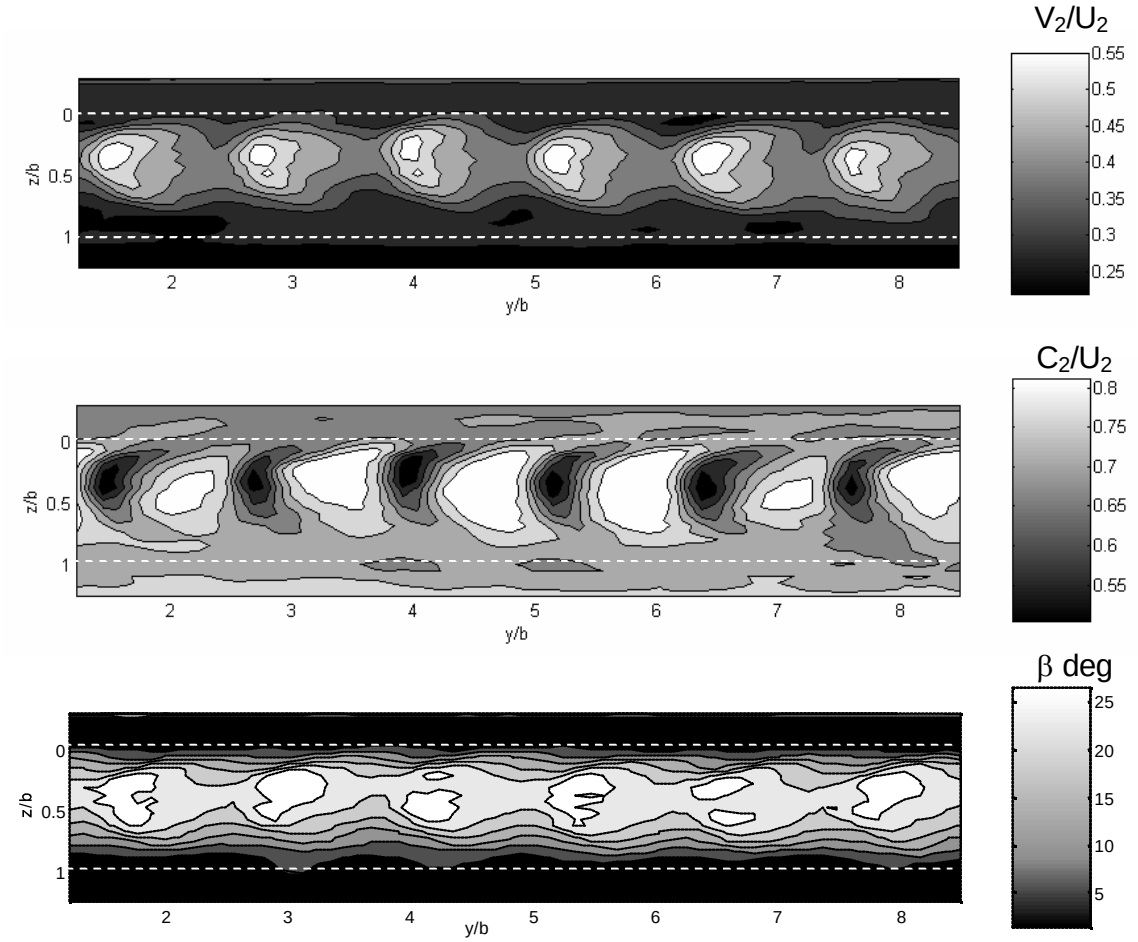

Figure 7 Passage-to-passage variation of (a) absolute velocity (b) relative velocity and (c) relative whirl angle. Rotor 2, 2250rpm at 2mm radial position.

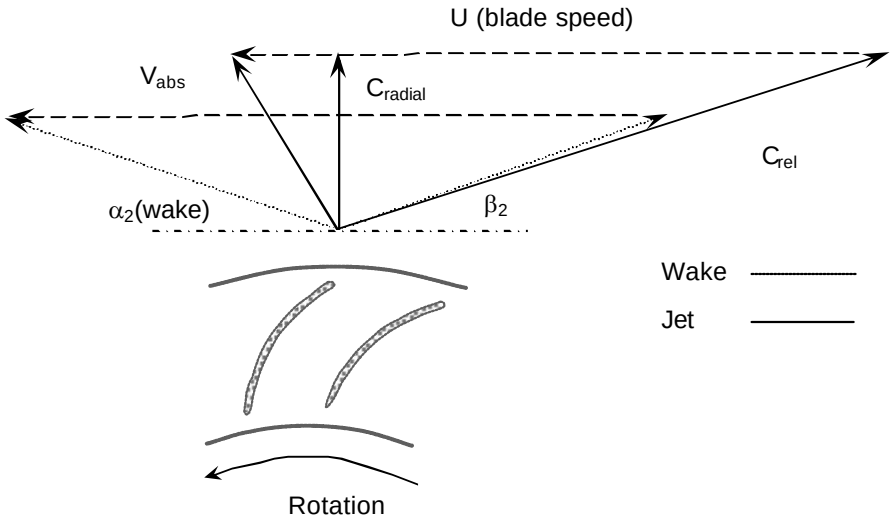

Figure 8Mid-span velocity triangles for Rotor 2 at 2250rpm showing the jet and wake regions.

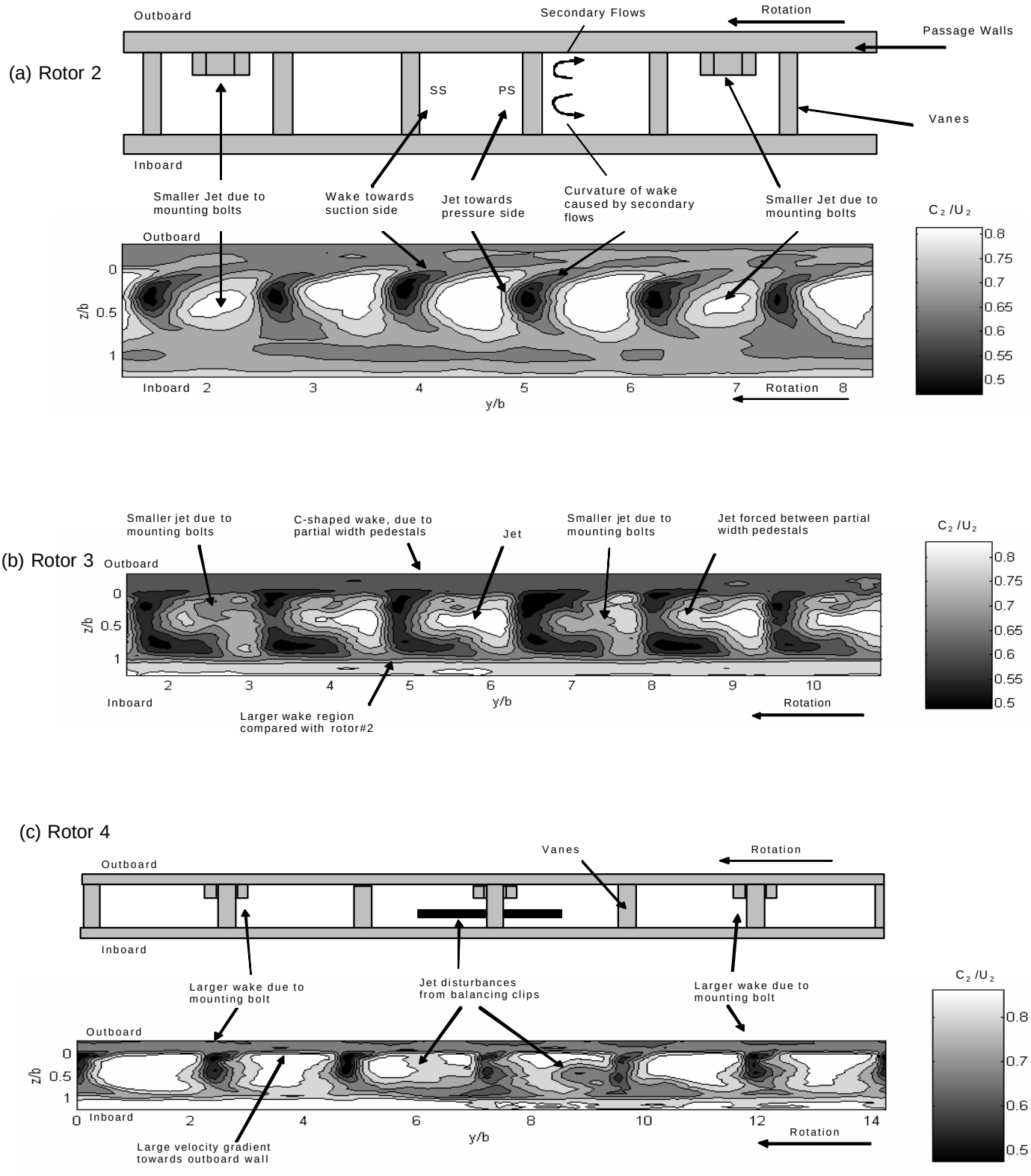

Figure 9 Relative velocity distributions for Rotors 2, 3 and 4. Measurements taken at 2mm from the exit plane with a rotational speed of 1500rpm (a) Rotor 2 (b) Rotor 3 (c) Rotor 4. Rotor 3 geometry cannot be shown due to confidentiality agreements.

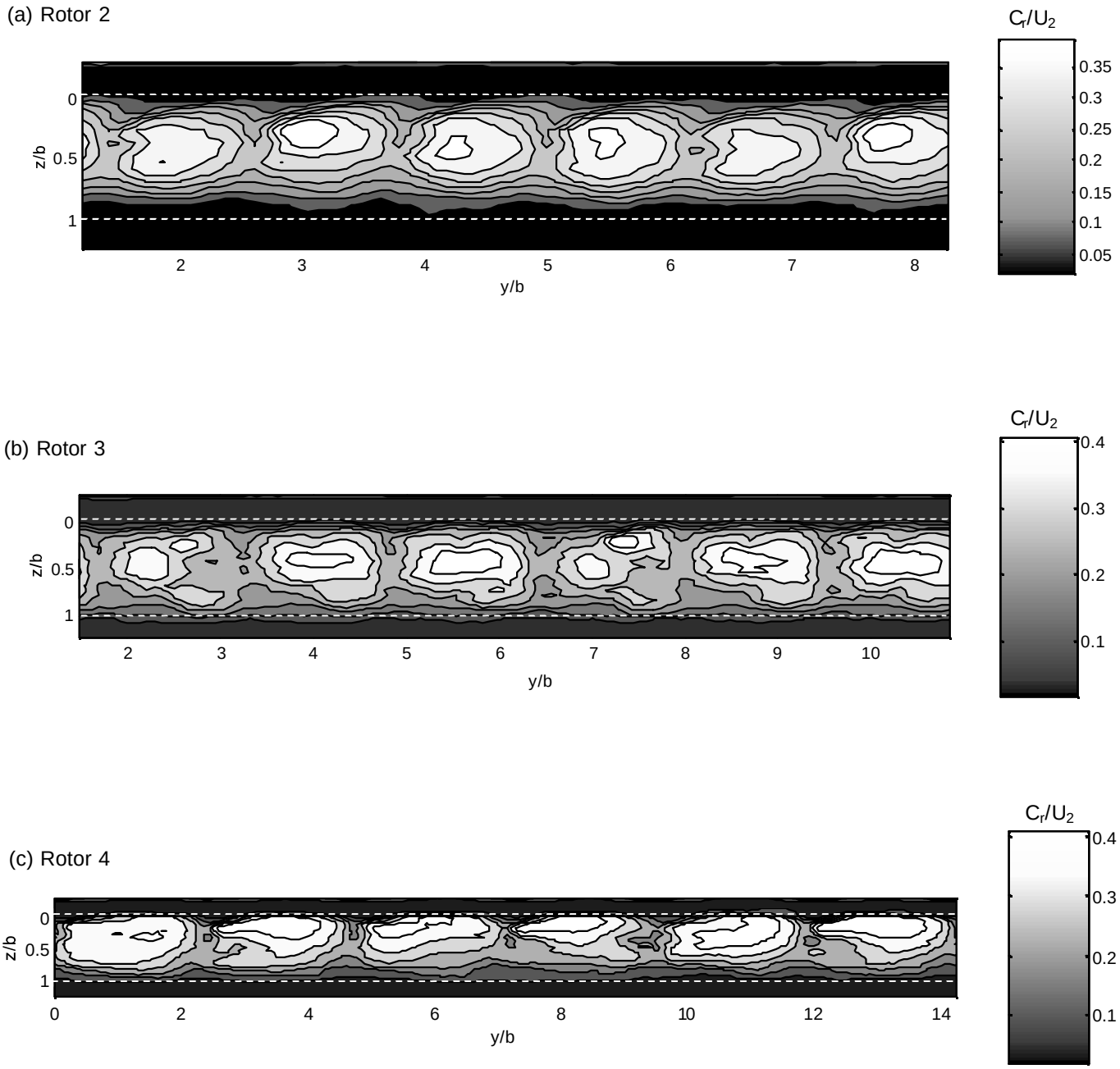

Figure 10 Radial velocity distributions for Rotors 2, 3 and 4. Measurements taken at 2mm from the exit plane with a rotational speed of 1500rpm (a) Rotor 2 (b) Rotor 3 (c) Rotor 4.

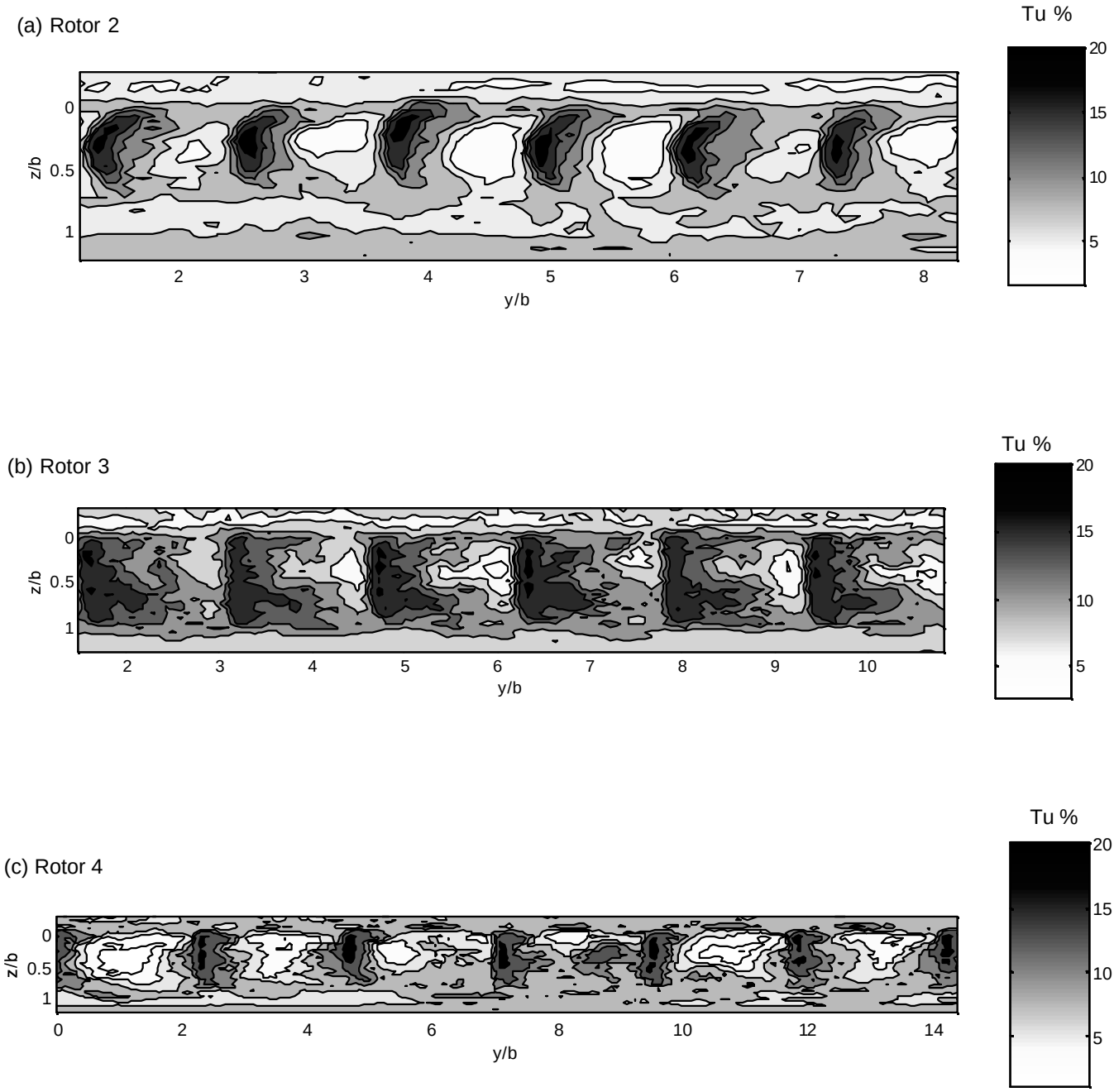

Figure 11 Turbulence intensity distributions for Rotors 2, 3 and 4. Measurements taken at 2mm from the exit plane with a rotational speed of 1500rpm (a) Rotor 2 (b) Rotor 3 (c) Rotor 4.

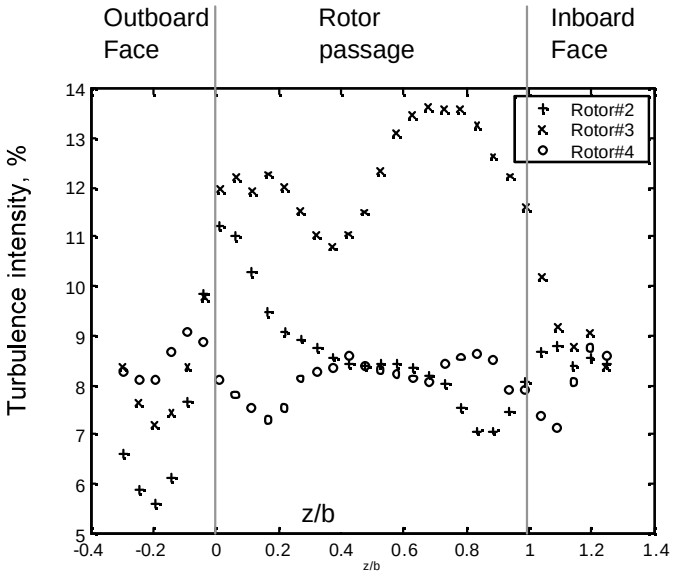

Figure 12 Circumferentially averaged turbulence intensity.

Rotors 2, 3 and 4. 2mm from the exit plane. 1500rpm.